Natural Resources for Human Health

eISSN: 2583-1194

Original Research

Received 01 July 2026
Revised 20 Aug 2026
Accepted 03 Sep 2026

Natural Resources for Human Health 2026, Vol. 6 (19s): 570–578

KEYWORDS:
Alzheimer research; graph signal processing; dispersion entropy; topology alignment; cross fitting; conditional stability.

Cross fitted topology alignment entropy for brain graph analysis in Alzheimer research

Dr. V. Sivabharathi[1], Nandhini J[2]*, Dr. K. Rajakumari[3], Arun A. N.[4]

[1]Associate Professor, Department of Mechanical Engineering, Sri Ramakrishna College of Engineering, Perambalur – 621213, Tamil Nadu, India.
Email and telephone: [to be supplied].
ORCID: [to be supplied].
[2]Assistant Professor, Department of Computer Science and Engineering, RMD Engineering College, Thiruvallur, Tamil Nadu, India.
Email: Nandhini.raman20@gmail.com; telephone: +91 6380386807.
ORCID: [to be supplied].
[3]Professor, Department of Computer Science and Engineering, PERI Institute of Technology (4115), No. 1, PERI Knowledge Park, Mannivakkam, West Tambaram, Chennai – 600048, Tamil Nadu, India.
Emails: rajakumari.k@peri.ac.in; krajikharsh24@gmail.com; telephone: +91 9941610588.
ORCID: [to be supplied].
[4]Associate Professor, Department of Computer Science and Engineering, Sri Venkateswara Institute of Science and Technology, Kolundhalur, Tiruvallur – 631203, Tamil Nadu, India.
Email: arun.svist.cse@gmail.com; telephone: [to be supplied].
ORCID: [to be supplied].
* Corresponding author (proposed): Nandhini J,

ABSTRACT: Entropy calculated after graph filtering depends on both signal dynamics and the graph estimated from those signals, complicating the interpretation of regional complexity in Alzheimer research. We introduce cross fitted topology alignment graph entropy (TAGE), which estimates a graph on one temporal segment and evaluates dispersion entropy on another. An alignment contrast compares the observed topology with node permutations that preserve its spectrum and edge-weight multiset. Three fixed filters sum to the identity, and a training-block bootstrap describes sensitivity to graph estimation. The reported synthetic audit includes five configurations, 80 recordings per configuration, and 99 graph permutations. For independent autoregressive signals, the mean low-band contrast decreased from 0.01057 with same-segment estimation to 0.00029 with cross fitting. Nevertheless, 11.25% of cross fitted ranks were at or below 0.05; this proportion increased to 26.25% under temporal heterogeneity. These findings support temporal separation as an audit of graph-dependent entropy while demonstrating that alignment ranks require further calibration. The study provides methodological and simulation evidence only; it does not establish an Alzheimer biomarker or patient-level diagnostic performance.

Natural Resources for Human Health

eISSN: 2583-1194

1 INTRODUCTION

Regional entropy is a simple summary of the temporal architecture of functional magnetic resonance imaging (fMRI) signals. This description is appealing in Alzheimer disease (AD) where altered dynamics could be associated with changes in functional coordination. It has been reported that there are differences in complexity between diagnostic groups by temporal multiscale entropy (Niu et al., 2018). Graph representations, which incorporate the spatial relations between regions, enable analysis of a signal with respect to a network instead of a set of independent time series (Hammond et al., 2011; Shuman et al., 2013).

Pu, Song, and Chai (2025) combined spectral graph wavelet filtering with multivariate dispersion entropy to examine differences between Alzheimer disease and healthy control groups. This motivates a distinction between graph frequency, which describes variation across connected regions, and temporal frequency, which describes variation over time. A low graph-frequency component is spatially smooth relative to a specified graph; it need not represent a slow temporal oscillation or healthier physiology.

An additional question concerns the graph itself. If functional connectivity is estimated from a finite recording, the filter is a function of that recording. Entropy subsequently calculated on the filtered recording inherits this dependence. This is an estimation issue even in an unsupervised analysis; it should not be confused with leakage of diagnostic labels. It is also different from asking whether an entropy estimator can distinguish two clinical groups.

This study asks whether lower entropy reflects reproducible alignment between signals and the named graph topology, beyond the effect of a filter with the same spectrum. We propose a contrast evaluated on held-out temporal segments and accompanied by a conditional description of graph stability. Synthetic signals provide a controlled setting for examining these distinctions before clinical interpretation.

The proposed method separates graph fitting from entropy evaluation, uses a spectrum-preserving alignment reference, and describes sensitivity through training-block resampling. Reconstruction and permutation properties provide implementation checks. The evidence is restricted to controlled stochastic signals; clinical validation remains future work.

1.1 Related work

Spectral graph wavelets are functions of a graph Laplacian (Hammond et al., 2011), within the broader framework of graph signal processing (Shuman et al., 2013). Dispersion entropy maps amplitudes into categories and quantifies the distribution of embedded patterns (Rostaghi and Azami, 2016). Extensions characterize irregularity using graph neighborhoods (Fabila-Carrasco et al., 2023), amplitude information in graph permutation entropy (Roy et al., 2026), and sample entropy for graph signals (Lei et al., 2026). TAGE addresses estimation and interpretation within this established family of approaches.

The motivating fMRI method (Pu et al., 2025) combines graph bands, regional neighborhoods, and multivariate dispersion entropy to compare clinical groups. TAGE changes the estimand: it quantifies temporal dispersion entropy at each filtered node and compares the named topology with isospectral relabelings. Neither TAGE nor its same-segment comparator is a reimplementation of the multivariate neighborhood estimator used by Pu et al. (2025).

1.2 Research gap

Entropy differences after graph filtering admit several explanations. Spatial mixing can alter temporal pattern distributions; finite-sample correlations can influence the estimated graph; and physiological coupling can align signals with connectivity. Regional differences in temporal dynamics can also produce alignment without interregional coupling. A scalar entropy value cannot distinguish these explanations.

The estimation question is therefore how to quantify topology-dependent entropy while separating graph fitting from evaluation and reporting graph sensitivity. Table 1 compares the stated analysis components; it does not imply that all graph-entropy studies share the same limitations.

Natural Resources for Human Health
eISSN: 2583-1194

Table 1. Comparison of analysis components

Component	Motivating analysis (Pu et al., 2025)	**TAGE**
Entropy input	Multichannel neighborhood signals	Filtered temporal signal at each node
Graph evaluation	Subject recording	Opposite temporal half
Reference	Clinical group comparison	Permuted graph with matched spectrum
Graph sensitivity	Parameter assessment	Training-block bootstrap
Evidence here	Published patient study	Executed simulations only

1.3 Interpretation of the reference

Node relabeling preserves the graph spectrum but changes which signals are associated with named neighborhoods. This reference addresses topology-signal alignment, not causation. It cannot separate preprocessing effects from physiological interactions, or temporal autocorrelation from heteroscedasticity. Motion can produce systematic functional connectivity artifacts (Power et al., 2012), which are not automatically removed by graph permutation.

2 MATERIALS AND METHODS

Figure 1 summarizes the processing pipeline and the separation of graph fitting from entropy evaluation.

2.1 Temporal separation and graph construction

Let $X \in \mathbb{R}^{N\times T}$ contain N regional signals. Remove a central guard of g frames to retain two contiguous segments A and B; the implementation uses g = 16. The first fold fits the graph on A and evaluates it on B, while the second fold swaps their positions. The guard is used to decrease the short-range dependence: it does not ensure the independence in a nonstationary or long-memory recording. The clinical censoring should not create artificial adjacent samples, and should be based on retained frame indices that are regularly sampled.

Using only the training half, center and scale each region. Apply the resulting parameters to the evaluation half. Estimate a Ledoit-Wolf shrinkage covariance (Ledoit and Wolf, 2004), convert it to a correlation matrix R, and define

$$W_{ij} = \max(R_{ij}, 0), \quad i \neq j; \qquad W_{ii} = 0. \quad (1)$$

No density threshold is selected from the data. The method intentionally discards negative correlations, so conclusions concern a positive connectivity graph. This restriction must be reconsidered for applications where anticorrelation is central. With $d_i = \sum_j W_{ij}$, set $q_i = d_i^{-1/2}$ for nonisolated nodes and zero otherwise. The normalized Laplacian is

$$L = \mathrm{diag}\{\mathbf{1}_{d_i>0}\} - QWQ, \quad Q = \mathrm{diag}\{q_i\}. \quad (2)$$

This convention assigns zero Laplacian rows to isolated nodes; numerically, degrees at or below 10^{-12} are treated as zero. Shrinkage is a numerical regularizer, not a proof that graph estimates from autocorrelated samples are unbiased.

2.2 Fixed graph filters

For $L = U\Lambda U^{\top}$, define three overlapping kernels on $\lambda \in [0,2]$:

$$g_0(\lambda) = e^{-4\lambda}, \quad g_1(\lambda) = e^{-\lambda} - e^{-4\lambda}, \quad (3)$$

$$g_2(\lambda) = 1 - e^{-\lambda}, \qquad F_k = U g_k(\Lambda) U^{\top}. \quad (4)$$

The terms low, middle, and high denote relative graph-spectral emphasis, not disjoint spectral intervals. The constants are fixed before simulation. All kernels are nonnegative and sum to one. Therefore,

Natural Resources for Human Health

eISSN: 2583-1194

$$F_0 + F_1 + F_2 = I, \qquad \sum_{k=0}^{2} F_k X = X. \quad (5)$$

This is an exact reconstruction identity; it is not an orthogonal decomposition or an energy-conservation identity. Filtered signals at a node remain temporal series, with spatial context introduced by F_k.

2.3 Held out dispersion entropy

For each graph, band, and region, estimate filtered training mean μ_{ki} and standard deviation σ_{ki}. Map evaluation samples to $c = 3$ classes through the standard normal cumulative distribution function Φ:

$$z_{ki,t} = \min\{c-1, \lfloor c\Phi\left((y_{ki,t} - \mu_{ki})/\sigma_{ki}\right)\rfloor\}. \quad (6)$$

Symbols are numbered from zero. With embedding dimension $m = 2$ and delay one, the pattern index is $cz_t + z_{t+1}$. If $p_{ki}(v)$ is its empirical distribution over c^2 possible patterns, normalized dispersion entropy is

$$H_{ki} = -\frac{\sum_{v=0}^{c^2-1} p_{ki}(v)\log p_{ki}(v)}{\log(c^2)}. \quad (7)$$

Use $0\log 0 = 0$. A filtered training standard deviation below 10^{-10} marks the band-node estimate as unsupported rather than assigning entropy zero. The plug-in estimator retains finite-sample bias; the null comparison does not guarantee its cancellation.

2.4 Topology alignment contrast

Draw M node permutations with permutation matrices P_b. Keep the signals and temporal ordering unchanged, but replace each observed filter by

$$F_k^{(b)} = P_b F_k P_b^{\top}. \quad (8)$$

Each relabeled graph retains the observed eigenvalues, edge-weight multiset, density, and degree multiset, but does not preserve the degree assigned to a particular anatomical region. For each relabeling, filtered training parameters and held-out entropy are recomputed using identical operations for the observed and reference paths.

Let $H_{ki}^{(f)}$ denote observed entropy in fold f and $H_{ki}^{(f,b)}$ the corresponding relabeled entropy. Define

$$\Delta_{ki} = \frac{1}{2}\sum_{f=1}^{2}\left[\frac{1}{M}\sum_{b=1}^{M} H_{ki}^{(f,b)} - H_{ki}^{(f)}\right]. \quad (9)$$

A positive contrast indicates lower temporal pattern entropy under the named topology than under the reference relabelings. This direction is specified before evaluation. Negative contrasts remain valid descriptive outputs. A band summary is $s_k = N^{-1}\sum_i \Delta_{ki}$. The same permutation is used in both folds to retain a paired reference.

For $\bar{H}_k = \frac{1}{2N}\sum_{f,i} H_{ki}^{(f)}$ and corresponding $\bar{H}_k^{(b)}$, report the lower-tail alignment rank

$$r_k = \frac{1 + \sum_{b=1}^{M} \mathbf{1}\{\bar{H}_k^{(b)} \le \bar{H}_k\}}{M+1}. \quad (10)$$

Equation (10) is a Monte Carlo alignment rank. Interpreting it as an exact hypothesis-test probability would require exchangeability of signal assignments throughout the estimation procedure. Regional heterogeneity, residual temporal dependence, and reuse of both signal halves can violate this condition. Ranks are therefore descriptive and do not imply clinical significance.

2.5 Conditional graph stability

Resample contiguous blocks jointly across nodes within each training half, refit the graph, and retain the opposite evaluation half unchanged. Repeat equation (9) with a fixed permutation bank. For B repetitions, report the central 95% empirical range and fraction of positive contrasts. The illustrated analysis uses B = 80, block length 12, and M = 39. Block resampling

preserves ordering within blocks (Lahiri, 2003). These summaries describe sensitivity to the training data conditional on fixed evaluation signals; they are not population confidence intervals, and their nominal coverage has not been established.

Algorithm 1 - Cross fitted topology alignment graph entropy

1. Split X into contiguous halves A, B with a guard.
2. Generate a reproducible bank of M node permutations.
3. For each direction $A \to B$ and $B \to A$, standardize using training parameters and fit W, L, F_k.
4. Evaluate the observed entropy using filtered training parameters.
5. Relabel F_k for every permutation; recompute training parameters and evaluate reference entropies.
6. Average paired fold contrasts; return regional Δ, band summaries s, and descriptive ranks r.
7. Optionally bootstrap training blocks and return conditional stability summaries.

2.6 Implementation cost and checks

Dense covariance estimation costs approximately $O(N^2T)$ per fold, and eigendecomposition costs $O(N^3)$. Applying M relabeled dense filters costs $O(KMN^2T)$, with K = 3. Equation (8) relabels precomputed operators, avoiding an eigendecomposition for every permutation. Bootstrap repetitions multiply this cost. Sequential permutation processing limits additional storage to approximately $O(KN^2 + KMN)$, apart from input signals and working arrays. The reported implementation checks concern reconstruction, symmetry, preservation of the spectrum under permutation, and seed determinism. Sparse polynomial approximation remains a future implementation option.

2.7 Controlled signal generators

No participant data were obtained or analyzed. Each configuration comprises 80 independent synthetic recordings with N = 24 nodes. Standard recordings have T = 272 samples: two 128-sample halves separated by a 16-frame guard. Short recordings have T = 140 samples and 62 samples per half. Each generator discards a 300-step burn-in.

For coupled signals, define a weighted graph W^* with three groups of eight nodes, within-group weight 0.8, between-group weight 0.03, and zero diagonal. Let $S = D^{-1/2}W^*D^{-1/2}$. Generate

$$x_t = (0.35I + 0.55S)x_{t-1} + \epsilon_t, \quad \epsilon_t \sim \mathcal{N}(0, I). \quad (11)$$

The spectral radius of the transition operator is at most 0.90. Independent signals use the transition operator 0.65I. Disrupted signals start from (11) and replace the first six outputs by $0.2x_i + 1.5\eta_i$, with independent white Gaussian η_i. A heterogeneous negative control is a control with independent signals whose first six nodes are substituted with independent white noise. In this way, there is no coupling between the different populations of activity nodes, and the time dynamics of the heterogeneous signals are different.

All configurations use $c = 3$, $m = 2$, delay one, and $M = 99$. Generator seeds are $10000 + j$ and permutation seeds $20000 + j$, for $j = 0, \ldots, 79$. The same-segment ablation fits and evaluates on the complete recording. It isolates an estimation choice within TAGE; it is not a benchmark against the published algorithm in (Pu et al., 2025). Low-band results are designated as the primary audit, and machine-readable outputs retain all three bands.

3 RESULTS AND DISCUSSION

3.1 Estimation dependence and heterogeneity

Table 2 summarizes the low-band contrasts. For independent signals, cross fitting reduced the mean contrast from 0.01057 to 0.00029, and the number of ranks at or below 0.05 fell from 70/80 to 9/80. The reported binomial 95% interval for 9/80 is 5.28%–20.28%, which does not support a claim of calibration at 5%. The threshold summarizes a calibration failure mode; it is not a clinical decision rule.

Table 2. Low-band contrast and descriptive rank frequency

Configuration	Cross fitted mean ± SD	Same segment mean ± SD	Rank ≤ 0.05 CF / SS
Independent	0.00029 ± 0.00710	0.01057 ± 0.00431	9 / 70
Coupled	0.00503 ± 0.01497	0.01307 ± 0.01225	25 / 44
Disrupted	0.02712 ± 0.01193	0.03508 ± 0.01025	63 / 79
Coupled short	0.00094 ± 0.02280	0.01568 ± 0.01346	13 / 39
Heterogeneous	0.00649 ± 0.00506	0.01216 ± 0.00444	21 / 74

Each frequency has denominator 80. CF denotes cross fitted; SS denotes same segment. These frequencies are not diagnostic accuracies.

Figure 2 shows the distributions of low-band contrasts and the descriptive rank frequencies across configurations.

3.2 Stability and failure modes

Coupled signals produced a positive mean cross fitted contrast with substantial between-recording variation. Shortening the recordings increased the standard deviation from 0.01497 to 0.02280. Disrupted signals produced a larger contrast than coupled signals, but this cannot be interpreted as stronger coupling or better health because replacement changes the balance of predictable and unpredictable temporal components. The uncoupled heterogeneous configuration yielded a mean contrast of 0.00649, with 21/80 ranks at or below 0.05. Thus, the present reference cannot distinguish physiological coupling from regional temporal heterogeneity.

Figure 3 describes conditional graph sensitivity in one coupled recording, using generator seed 12345 and bootstrap seed 54321. Node indices have no anatomical interpretation. Reconstruction and permuted-spectrum errors were both 8.88×10^{-16}, establishing implementation consistency rather than empirical validity.

3.3 Clinical validation and future work

Cross fitting reduced the mean alignment contrast for homogeneous independent signals, while short recordings showed greater variability. Spectrum-preserving relabeling controls the graph filter spectrum but changes the topology-signal assignment; it does not guarantee a calibrated null test. Future references should account for regional temporal spectra or prespecified dynamics strata and be assessed through additional null simulations. Clinical validation would require preprocessing and graph parameters to be fixed before examining diagnostic outcomes, with documented eligibility, participant independence, motion, scanner characteristics, and cognitive assessments. ADNI is a possible cohort, subject to its access requirements (Alzheimer's Disease Neuroimaging Initiative, 2026). Group effects and regional analyses should account for repeated and dependent measurements. Benjamini-Hochberg false discovery rate control requires appropriate dependence assumptions (Benjamini and Hochberg, 1995). Findings should be replicated in an independent sample. Any predictive extension would require feature selection and tuning within training folds and nested evaluation (Varma and Simon, 2006). No patient analysis is reported here.

4 CONCLUSIONS

TAGE combines a topology-alignment entropy contrast with conditional graph-stability summaries. In the reported simulations, temporal separation reduced but did not eliminate rank distortion. Regional temporal heterogeneity limits interpretation of alignment as physiological coupling. Further calibration and independent clinical validation are necessary before assessing biomarker relevance or diagnostic utility.

Natural Resources for Human Health

eISSN: 2583-1194

Declaration of generative AI use

OpenAI ChatGPT assisted with the methodological concept, drafting, reference searching, and generation of implementation and plotting code, as disclosed in the source manuscript. It also assisted with language editing and journal formatting. The source manuscript reports that generated code was executed to obtain the synthetic results. The authors are responsible for independently verifying the analysis, references, originality, and conclusions. Tool version and dates of use: [authors to supply].

Acknowledgements

[Authors to confirm any non-author assistance or state that there are no acknowledgements.]

Funding

[Authors to provide funding sources, grant numbers, and recipient authors, or confirm that no specific funding was received.]

Author contributions

[Authors to confirm individual contributions using CRediT roles. Contributions have not been inferred from author order or designation.]

Conflicts of interest

[Each author to disclose relevant interests or confirm that no conflicts of interest exist.]

Ethics statement

This study reports synthetic simulations only. No human participants, patient records, or animal data were analyzed. Institutional requirements concerning exemption or approval should be confirmed by the authors.

Data and code availability

[Authors to provide an accessible repository or supplementary files containing the simulation code, synthetic outputs, plotting code, software versions, and instructions needed to reproduce the reported results.]

REFERENCES

[1] Alzheimer's Disease Neuroimaging Initiative, 2026. I am a researcher; how do I access ADNI research data or samples? https://support.adni4.org/hc/en-us/articles/31090030057236-I-am-a-researcher-how-do-I-access-ADNI-research-data-or-samples (accessed 8 October 2026).

[2] Benjamini, Y., Hochberg, Y., 1995. Controlling the false discovery rate: A practical and powerful approach to multiple testing. Journal of the Royal Statistical Society Series B 57(1), 289–300. https://doi.org/10.1111/j.2517-6161.1995.tb02031.x.

[3] Fabila-Carrasco, J.S., Tan, C., Escudero, J., 2023. Dispersion entropy for graph signals. Chaos, Solitons & Fractals 175, 113977. https://doi.org/10.1016/j.chaos.2023.113977.

[4] Hammond, D.K., Vandergheynst, P., Gribonval, R., 2011. Wavelets on graphs via spectral graph theory. Applied and Computational Harmonic Analysis 30(2), 129–150. https://doi.org/10.1016/j.acha.2010.04.005.

[5] Lahiri, S.N., 2003. Resampling Methods for Dependent Data. Springer, New York. https://doi.org/10.1007/978-1-4757-3803-2.

[6] Ledoit, O., Wolf, M., 2004. A well-conditioned estimator for large-dimensional covariance matrices. Journal of Multivariate Analysis 88(2), 365–411. https://doi.org/10.1016/S0047-259X(03)00096-4.

[7] Lei, M.-S.M., Fabila-Carrasco, J.S., Escudero, J., 2026. Sample entropy for graph signals: An approach to nonlinear dynamic analysis of data on networks. Nonlinear Dynamics 114, 1036. https://doi.org/10.1007/s11071-026-12885-y.

[8] Niu, Y., Wang, B., Zhou, M., Xue, J., Shapour, H., Cao, R., Cui, X., Wu, J., Xiang, J., 2018. Dynamic complexity of spontaneous BOLD activity in Alzheimer's disease and mild cognitive impairment using multiscale entropy analysis. Frontiers in Neuroscience 12, 677. https://doi.org/10.3389/fnins.2018.00677.

[9] Power, J.D., Barnes, K.A., Snyder, A.Z., Schlaggar, B.L., Petersen, S.E., 2012. Spurious but systematic correlations in functional connectivity MRI networks arise from subject motion. NeuroImage 59(3), 2142–2154. https://doi.org/10.1016/j.neuroimage.2011.10.018.
[10] Pu, R., Song, X., Chai, L., 2025. Graph signal entropy for analyzing functional brain abnormalities of Alzheimer's disease patients. IEEE Transactions on Neural Systems and Rehabilitation Engineering 33, 4112–4123. https://doi.org/10.1109/TNSRE.2025.3620444.
[11] Rostaghi, M., Azami, H., 2016. Dispersion entropy: A measure for time-series analysis. IEEE Signal Processing Letters 23(5), 610–614. https://doi.org/10.1109/LSP.2016.2542881.
[12] Roy, O., Campbell-Cousins, A., Fabila-Carrasco, J.S., Parra, M.A., Escudero, J., 2026. Activated permutation entropy for graph signals. Nonlinear Dynamics 114, 1107. https://doi.org/10.1007/s11071-026-12949-z.
[13] Shuman, D.I., Narang, S.K., Frossard, P., Ortega, A., Vandergheynst, P., 2013. The emerging field of signal processing on graphs: Extending high-dimensional data analysis to networks and other irregular domains. IEEE Signal Processing Magazine 30(3), 83–98. https://doi.org/10.1109/MSP.2012.2235192.
[14] Varma, S., Simon, R., 2006. Bias in error estimation when using cross-validation for model selection. BMC Bioinformatics 7, 91. https://doi.org/10.1186/1471-2105-7-91.

Figure legends

Figure 1. TAGE processing pipeline. Graph fitting uses a training half; entropy evaluation uses the opposite half. Permuted filters retain the graph spectrum. The procedure is repeated with the halves exchanged.

Figure 2. Executed synthetic audit. (a) Low-band contrasts, with interquartile boxes and whiskers extending to 1.5 times the interquartile range; outliers are omitted visually. (b) Observed descriptive rank frequencies. The dashed 0.05 line is a reference level, not evidence of valid test calibration.

Figure 3. Conditional graph stability in one synthetic coupled scan. (a) Mean contrasts and central 95% bootstrap ranges. (b) Fractions of positive contrasts across 80 graph-training bootstraps. Evaluation signals are fixed throughout.

Figure 1

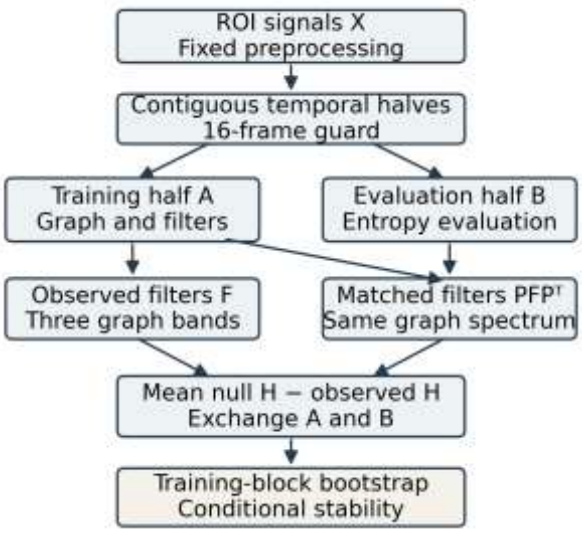


Figure 2

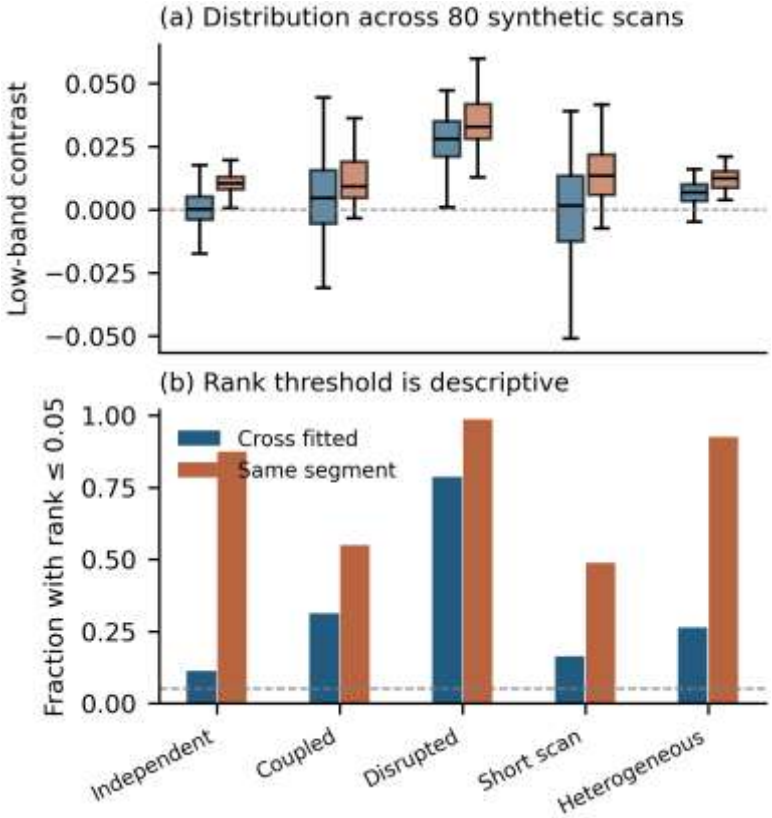


Figure 3

